Microstructure-based alloy compression strengthening model of an equiatomic high-entropy alloy CoCrFeNiNb

M. Cabibbo, F. Průša, S. Spigarelli, E. Santecchia, C. Paoletti

High-entropy alloys within the scientific community was promoted due to their exceptionally high mechanical and physical properties, namely compression strength, toughness, plasticity, hardness, wear, corrosion resistance, and thermal stability. In the present study, an equiatomic CoCrFeNiNb HEA was prepared by a sequence of conventional induction melting, powder metallurgy, and compaction via spark plasma sintering. The as-cast HEA showed an ultimate compression strength (UCS) of ~1400 MPa. After sintering and compaction at 1273K the UCS increased considerably up to ~2400 MPa. After compaction at 1273K the fcc phase was characterized by a diffuse presence of nano-size twinning. Extensive TEM quantitative analyses were carried out to model the UCS by the most significant microstructure strengthening features. A quite good agreement between the microstructure-strengthening model and the experimental UCS was found.

PAROLE CHIAVE: HIGH-ENTROPY ALLOYS (HEA), POWDER METALLURGY (PM), SPARK PLASMA SINTERING (SPS), MECHANICAL PROPERTIES, TEM, STRENGTHENING MECHANISMS

INTRODUCTION

High-entropy alloys (HEAs) belong to the group of modern metallic materials that have been intensively studied since 2004, when Cantor *et al.* reported the first CoCrNiFeMn high-entropy alloy [1]. HEAs generally consist of five or more principal metallic elements whose individual concentration can vary from 5 to 35 at. % [2]. The worldwide attention cast on these new alloys is chiefly due to their unique combination of properties, such as high strength [3], high toughness together with high plasticity [4], high hardness [2], excellent thermal stability [2], wear [5] and corrosion resistance [5,6]. Such unique properties are directly associated to the high configurational entropy of mixing, sluggish diffusion and severe lattice distortion [7].

HEAs are mostly strengthened by solid solutions and secondary phase induced precipitation. With this respect, niobium addition to HEAs (namely 5-emenet HEAs) is known to improve the alloy ductility and strength [4,8]. Both the mechanical properties are likely to be promoted by Nb addition due to its larger atomic radius compared to the usual elements constituting the 5-element HEAs.

On the other hand, Nb has negative enthalpies of mixing with Co, Fe, Cr and Ni [8] and forms Nb-enriched Laves phases [9]. Laves phases have hcp crystallographic structure, which substantially increases the yield, fracture strength, and the elastic modulus as it precipitates within the fcc matrix [9,10].

Marcello Cabibbo, Stefano Spigarelli, Eleonora Santecchia, Chiara Paoletti
DIISM / Università Politecnica delle Marche, Ancona, Italy - corresponding author (Marcello Cabibbo): e-mail m.cabibbo@staff.univpm.it; Tel. 0712204728

Filip Průša
University of Chemistry and Technology, Prague, Department of Metals and Corrosion Engineering, Prague 6, Czech Republic.

The amount of Laves phases increases with niobium content [10]. However, alloy plasticity tends to reduce by increasing in volume fraction of Laves phases [9]. Published results on HEAs [11] showed that only by balancing the Nb content in the alloy the strength and ductility can be improved.

HEAs are usually produced by combining mechanical alloying (MA) and consolidation process. This process combination guarantees the optimization of the alloy mechanical properties, which cannot be obtained by any other single conventional method [3,12,13]. One of the most used and sound consolidation method is the spark plasma sintering (SPS). In fact, the mechanical properties of HEAs prepared by combining MA and SPS were found significantly higher than those of as-cast alloys, chiefly due to the formation of a refined nanocrystalline microstructure [13,14].

In this work, high-entropy equiatomic CoCrNiFeNb alloys were prepared by a combination of short-term (8h) MA followed by compaction via SPS. The results showed an ultrafine-grained microstructure composed of fcc solid solution strengthened by hcp Laves phases as well as Cr_2O_3 nanocrystalline particles. The obtained microstructure resulted in excellent mechanical properties that outperformed the properties of the as-cast counterpart and were retained even when the material was exposed to temperatures up to 900K. A microstructure-based strengthening model was applied to describe the different features contributing to the showed extraordinary alloy compression strength.

EXPERIMENTAL PROCEDURES AND METHOD

The equiatomic CoCrNiFeNb alloy was prepared by mixing pure powders in equiatomic ratios and forming a 20 g powder batch that was eventually homogenized for at least 5 min. Mixture was done by AISI420 balls with addition of 5 wt.% of n-heptane as a process control agent (PCA). The mould was sealed and flushed with argon (purity of 99.996%) for at least 3 min with a flow rate of 3 cl/s. The mechanical alloying (MA, Retsch™ PM100®, Haan, Germany) was performed at a speed of 400 rpm in 30 min intervals followed by 10 min breaks to allow alloys cooling for a overall duration of 8h. The powdered alloy was then compacted by a spark plasma sintering (SPS, FCT-System™, HP- D10®, Frankenblicke, Germany) using a die, pistons and sealing papers all made of graphite. The process heating rate was 200K/min, and samples were compressed at 48 MPa. Compacted samples were 4 mm-thick with a diameter of 20 mm.

Microstructure inspections were carried out by transmission electron microscopy (TEM, Philips™ CM-200®) using a voltage of 200 keV and equipped with a double-tilt specimen holder and a liquid N2 cooling stage. TEM samples were prepared by grinding, polishing and dimpling 3 mm discs. The final preparation for electron transparency was carried out in a precision-ion milling system (PIPS, Gatan™) in a vacuum at a voltage of 12 V and with a tilting incident angle of 8° for the first half, 6° for the following quarter, and 4° for the final quarter of the whole Ar-ion thinning time. The statistical data were obtained by 3 different TEM discs. TEM analysis was carried out on the MA+SPS at 1273K condition. All statistical evaluations of the microstructure features used for the strengthening model were carried out by stereological methods according to ASM EN-112.

Two-beam excitation conditions were selected for most of the TEM observation and dislocation characterizations. Tangled dislocation (TD) density, ρ_{TD}, was quantified using Ham's interception stereological methods [15]. Thence, ρ_{TD} was calculated through the count of interception points between the mesh and the existing dislocations, n_{disl}, in the TEM micrographs. This was evaluated by $\rho_{TD} = 2n_{disl}/(l_{mesh}t_{TEM})$, were, l_{mesh} is the total length of the mesh, and t_{TEM} is the thickness of the TEM foil. Crystal thickness, t_{TEM}, was determined through the diffracted beam intensity variation under dual beam conditions, using converged electron beam diffraction (CBED) patterns. This way, by plotting the linear interpolation of data points in a $S^2/n_{fringes}^2$ vs. $n_{fringes}^{-2}$ graph, where S is the fringes spacing and $n_{fringes}$ the number of counted fringes, t_{TEM}^{-2} was determined at y-axis line intercept. The error due to the invisible dislocations (i.e., the ones oriented as to have $b \cdot g = 0$, where b is the Burgers vector and g refers to the dislocation lying crystallographic plane) is within the experimental error of the foil thickness evaluation.

The mechanical properties were determined by compression stress-strain tests carried out at room temperature, 1073K, and 1273K. Rectangular gage samples with length 1.5 times the side dimension were used. The compression tests were carried out on STM Labortech™, LabTest SP 250.1-VM® with a strain speed of 10^{-4} s^{-1} using at least three samples.

RESULTS AND DISCUSSION

Alloy microstructure

Figure 1 shows a representative BF-TEM micrograph of the alloy compacted at 1273K in which the three different constituents can be easily recognized: fcc matrix, hcp Laves

phases and rounded oxide particles. The three phases were crystallographically identified by means of selected area electron diffraction patterns (SAEDPs). These are fcc identified as γ-like phase characterized by a diffuse presence of tangled dislocations and twinning, a hcp Laves phase, and hcp Cr_2O_3 intergranular rounded oxides. The grains of the FCC phase showed the presence of lattice defects, mainly composed of dislocation pile-ups found in the solid solution, deformation nanotwins, and to some extent, the presence of secondary phase particles. The presence of stacking faults as well as nanotwins was also reported elsewhere [16,17]. The Laves lattice is a Co_2Nb-type structure, with crystallographic parameters a = 0.4835 nm and c = 0.7860 nm. As for the chemical composition of the Laves phase, Jiang *et al.* [10] reported the composition of this Laves phase as $Co(Ni,Fe,Cr)_2Nb$, while Liu *et al.* [18] reported a slightly different composition of $(Co,Fe,Ni)_2(Cr,Nb)$. Triple grain junctions were characterized by a diffuse presence of small rounded Cr_2O_3 oxides having an average diameter of 100 nm. Anyhow, the volume fraction of these oxides was quite low, being within the 1.5 vol.%.

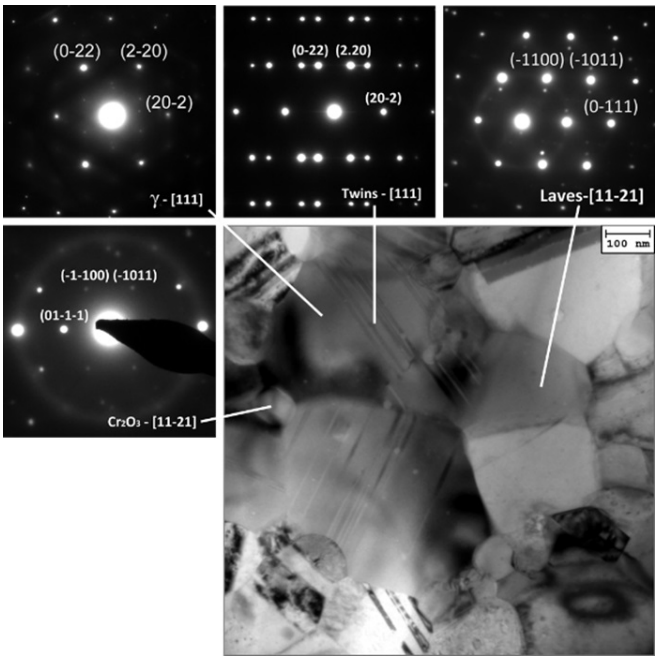

Fig.1 - BF-TEM micrographs of the 8h MA+SPS alloy compacted at 1273K; SAEDPs refer to the fcc γ phase (and twinned double spots), hcp Laves phase, and hcp Cr_2O_3 oxides (after M. Cabibbo *et al.*: J All Compd 835 (2020) 155308).

Mechanical properties

The mechanical properties of the as-cast alloy and the MA+SPS compacted alloy are reported in Figure 1, while the corresponding compression curves are reported in the Figure 2.

The here reported mechanical properties of the HEA are quite interesting as the alloy reached a quite high compression strength of almost 2300 MPA, with a close yield strength of about 2200 MPa. These results are considerably higher than those reported by Qin *et al.* [9] in a similar $(CoCrCuFeNi)_{100-x}Nb_x$ (x=0-16) alloy prepared by arc melting, where a maximum value of 1322 MPa was reached and corresponded to the $(CoCrCuFeNi)_{84}Nb_{16}$ alloy. In this latter case, the alloy microstructure was composed of fcc solid solution up to a content of 8 at.% Nb. It resulted that the observed high UCS values obtained after MA+SPS at 1273K were induced by solid solution strengthening of the fcc matrix, due to Nb, as well as the significant volume fraction of the Laves phases.

The here reported mechanical properties of the HEA are quite interesting as the alloy reached a quite high compression strength of almost 2300 MPA, with a close yield strength of about 2200 MPa. These results are considerably higher than those reported by Qin *et al.* [9] in a similar $(CoCrCuFeNi)_{100-}$

$_xNb_x$ (x=0-16) alloy prepared by arc melting, where a maximum value of 1322 MPa was reached and corresponded to the $(CoCrCuFeNi)_{84}Nb_{16}$ alloy. In this latter case, the alloy microstructure was composed of fcc solid solution up to a content of 8 at.% Nb. It resulted that the observed high UCS values obtained after MA+SPS at 1273K were induced by solid solution strengthening of the fcc matrix, due to Nb, as well as the significant volume fraction of the Laves phases.

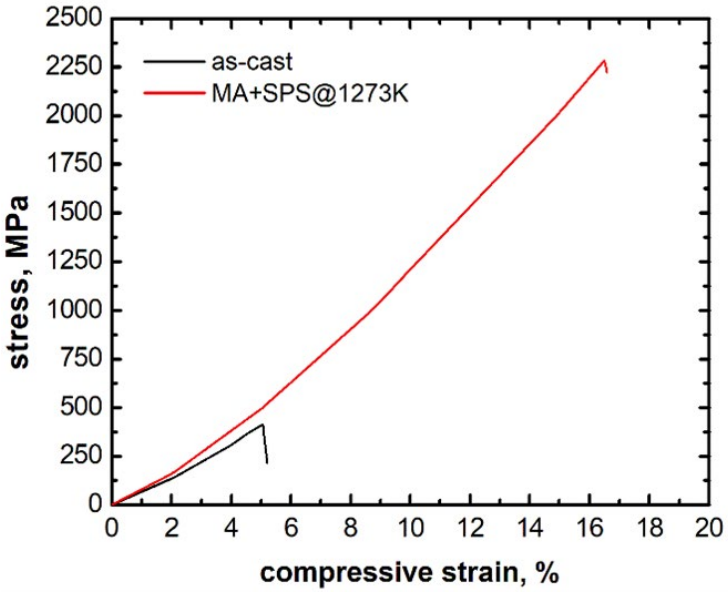

Fig.2 - Compressive stress-strain curves at room temperature of the equiatomic MA+SPS CoCrFeNiNb alloy compacted at 1273K, and compared to the results obtained in the as-cast alloy.

Tab.1 -Compression mechanical properties of the equiatomic CoCrFeNiNb HEA. YCS is the yield compressive strength; UCS is the ultimate compressive strength.

HEA exp conditon	Test temperature, K	YCS, MPa	UCS, MPa
8h MA+SPS at 1273K	873	2178	2284

It should be noted that a simple substitution of Mn by Nb in the investigated MA+SPS alloys resulted in a tremendous increase in the compressive properties when compared to the results of our previous research that focused on equiatomic CoCrFeNiMn alloys [14]. On the other hand, the UCS increase corresponded to a significant microstructural refinement that involved grain boundary strengthening, solid solution strengthening and strengthening through the hcp Laves phases homogeneously distributed in the alloy. These observations are in good agreement with other published works [10,18].

Thus the strengthening of the present HEA is driven by the three cooperating microstructure factors: fcc Nb solid solution, matrix grain refinement and twinning, and Laves phase formation.

Microstructure strengthening model

The different microstructure strengthening contributions are attributed to the three alloy constituents, i.e., the γ-phase, the Laves phase, and the Cr_2O_3 oxide particles. The γ-phase is strengthened by Hall-Petch mechanism (grain boundary), solid solution, tangled dislocations, secondary phase particle, and twinning formation. Lattice friction strength of the unreinforced alloy, σ0, was assumed to be as the one of pure cobalt σ0 ≅ 255 MPa [19]. The overall microstructure strengthening was evaluated by the rule of mixtures of the different contributors, according to [20].

Thence, the different strengthening phases and interphase constituents were combined as sum of squares, Eq. (1):

$$[1]\quad \sigma_y\,(CoCrFeNiNb\text{-}HEA) = \sigma_0 + \sigma_{ss} + \sigma_d + \sigma_{HP} + \sigma_T + \sigma_{ssp} + \sigma_P = \sigma_0 + \{[V_V^{\gamma}(\sigma_{ss} + \sigma_d + \sigma_{HP} + \sigma_{spp} + \sigma_T)]^2 + [V_V^{Laves}(\sigma_{TE}^{Laves} + \sigma_{LT}^{Laves}) + V_V^{Cr2O3}(\sigma_{TE}^{Cr2O3} + \sigma_{LT}^{Cr2O3})]^2\}^{0.5}$$

where σss is the strengthening contribution from solute atoms (solid solution strengthening) which only pertains to the γ-phase, σd is the strengthening contribution from tangled dislocations within the γ grains, σ_{HP} is the γ-grain contribution determined by the Hall-Petch relationship between grain size (Dγ) and alloy strengthening contribution, σ_T represents the twinning contribution to the alloy strength, σ_{ssp} and σ_P are the strengthening contribution from secondary-phase particles within the γ-phase (shearable) and from coarser intergranular particles (non-shearable), i.e., Laves and Cr_2O_3, respectively. According to these two coarser intergranular particles, the σ_P in Eq.(1) yields a strengthening contribution constituted by a linear sum of the Orowan (bypass) strength, σ_{OR}, particle thermal expansion, σ_{TE}, and related thermal expansion between the particles and the surrounding matrix, σ_{LT}.

The volume fractions of the three phases, namely V_v^{γ}, V_v^{Laves}, and V_v^{Cr2O3}, were determined by stereological methods (ASM EN-112), and related data are reported in Table 2.

In the following, all the meaningful strengthening terms are calculated.

Solid solution strengthening

Substitutional solid solution strengthening model, based on dislocation-solute elastic interactions can be here applied limited to the two major solute elements, Cr and Nb. The dislocation-solute elastic interaction is primarily attributed to atomic size differences among the solute atoms and the elements constituting the bulk of the existing phases, i.e. the γ-phase [21]. The atomic radii (Å) of the HEA constituting elements are Co (1.26), Cr (1.66), Fe (1.27), Ni (1.25), and Nb (1.98). According to [21] and references therein, the solute strengthening contribution essentially comes from those elements having a significant atomic size difference with respect to cobalt that constitute the γ-matrix. Thence, the Cr and Nb alloy solute strengthening contribution is estimated by Eqs. (2a) and (2b) [22]:

$$\sigma_{ss}(Cr) = MGb\varepsilon_s^{1.5}Cr^{0.5} \quad [2a]$$

$$\sigma_{ss}(Nb) = MGb\varepsilon_s^{1.5}Nb^{0.5} \quad [2b]$$

where M = 3.06 is the Taylor factor, G is the shear modulus, which for the equiatomic CoCrFeNiMn HEA was set to 74 GPa, b = 0.255 nm is the Burger's vector, ε_s refers to the atomic size mismatch of respectively Cr and Nb respect to the Co-matrix (i.e. γ-phase). It resulted that, according to Eq. (2), the solid solution strengthening contribution yield by Nb is expected to be in excess of the ratio of Nb/Cr atomic radius (=1.98/1.66). Anyhow, it is hard to determine a quantitative value for the two element concentration within the γ-phase. Thence, in order to estimate this strengthening contribution, He *et al.* [23] in a study of a similar but not exactly the same HEA, showed that, in most of the experimental cases of HEAs, the solute strengthening contribution can be estimated as no higher than 25 MPa for each meaningful element. That is, in the present case, a value within 40-45 MPa can be considered as a realistic strengthening estimation. This appears to be quite low compared to the overall compression yield stress, experimentally evaluate to be $\sigma_y \cong 2300$ MPa.

Dislocation strengthening

Tangled dislocation strengthening was calculated by Eq. (3):

$$\sigma_d = M\alpha Gb(\rho_d^{0.5}) \quad [3]$$

where, for the FCC γ-phase, α = 0.2 [24]. The tangled dislocation density within the γ-phase was measured with a stereological method by counting dislocation ends that intercepted equal radius circles in 15 different TEM micrographs and for more than 50 γ grains. The tangled dislocation distribution within the γ grains was revealed by tilting the sample to align the beam to the γ_{111} zone axis. The mean dislocation density, $\rho_{dislocation}$, is reported in Table 2, and the related statistical data are shown in a plot reported in Figure 3. The dislocation strengthening calculated by Eq. (3) was $\sigma_d = 310 \pm 20$ MPa.

Grain boundary (Hall-Petch) strengthening

Figure 3 reports the statistical data of the mean γ grain size, and the mean equivalent diameter was Dγ = 180 ± 20 nm. Thus, Hall-Petch strengthening was given by Eq. (4):

$$\sigma_{HP} = k_{HP}(D_{\gamma})^{-0.5} \quad [4]$$

where, k_{HP} is the Hall-Petch constants, in this case for nanocrystalline grains D_γ. This is known to be significantly smaller than the values generally used for the coarse-grained counterparts (typically micrometre-scale grains). In this regard, several studies have shown that a number of alloy physical and mechanical parameters of CoCrFeNiNb, CoCrFeNiMn, and other Co-based HEAs are similar to those of micrometer and
submicrometer-size grained pure Fe [21,25]. On the other hand, the Hall-Petch constant k_{HP} can vary significantly in complex alloy systems such as the HEAs [14,26]. In fact, Shaysultanov *et al.* [26] for their strengthening model of a similar CoCrFeNiMn equiatomic HEA use a k_{HP} = 0.35 MPa·m$^{1/2}$ (350 MPa·m$^{1/2}$). Compared to this value for k_{HP}, a significantly lower value, k_{HP} = 200 MPa·μm$^{1/2}$, was used for a similar CoCrFeMnNi HEA in [27], while a slightly higher value, k_{HP} = 400 MPaμm$^{1/2}$, was used for a C-added CoCrFeNiMn HEA in [28]. On the other hand, in a number of published works on quite similar CoCrFeNiMn HEA [29-33], k_{HP} was set at 490 MPa·μm$^{1/2}$. In a similar CoCrFeNiMn [34] and a quaternary CoCuMnNi HEA [35], k_{HP} = 494 MPa·μm$^{1/2}$. Even higher values were reported in some other published works. For instance, Zhao *et al.* [36] reported a k_{HP} = 568 MPa·μm$^{1/2}$ to model a CoCrNi medium-entropy alloy, while Sun *et al.* [37] presented a more comprehensive work on temperature-dependent Hall-Petch relationship in a CoCrFeNiMn HEA. They found that a general trend of k_{HP}(T) = 659-0.39T, with temperature, T, in K. That is, a k_{HP}(T=25K) = 650 MPa·μm$^{1/2}$. High Hall-Petch constants were also reported in [38] k_{HP} = 550 MPa·μm$^{1/2}$, for a Cr-rich CoCrFeMnNi HEA, and a value of k_{HP} = 667 MPa·μm$^{1/2}$ was used in [39] for a CoCrFeNiMn HEA, and similarly in [40] for a different FeCrNiCoMn HEA. With this significant variety of Hall-Petch constant used for similar equiatomic 5-element HEAs, the right value to use is somehow not straightforward. Yet, since in most of the recent literature works on modelling of similar equiatomic HEAs a value of k_{HP} = 400 MPaμm$^{1/2}$ was used [29-33], this was here considered as the most appropriate value. Having said that, the Hall-Petch strengthening contribution yield by the γ-phase was calculated as σ_{HP} = 940 ± 50 MPa.

Twin strengthening

Twin boundaries, σ_T, was calculated by a Hall-Petch type relationship as follows [41], Eq. (5):

$$\sigma_T = k_{TB}(\lambda_{TB})^{-0.5} \quad [5]$$

where, k_{TB} is a Hall-Petch type constant equivalent to the Hall-Petch constant for nanocrystalline γ grains, $k^{nc-\gamma}{}_{HP}$, and λ_{TB} is the average twin boundary (TB) spacing. In Eq. (6) k_{TB} = 35 MPa·μm$^{1/2}$. The TB spacing was statistically evaluated with 20 high-magnification TEM micrographs that contained more than 100 individual γ grains and whose distribution is shown in the plot of Figure 3. The related mean value was λ_{TB} = 11.0 ± 2.5 nm, as reported in the Table 2. That is, the mean twin strengthening contribution was calculated to be σ_T = 340 ± 40 MPa.

3.3.5. Secondary phase particle (shearable) strengthening

The γ-phase was also strengthened by the existing secondary phase particles. These were quite small and round-shaped, with mean equivalent diameter, d_{spp} = 7.5 ± 0.5 nm, a mean spacing, λ = 23 ± 3 nm, and a volume fraction, V_v^{spp} = 1.2 ± 0.2% of the V_v^{γ}. Based on well-established models of strengthening from secondary phase particles ([20] and references therein), it can be assumed that the secondary phase particles have a mean diameter corresponding to a typical dislocation strengthening mechanism of bowing, which, according to [20,42], can be calculated by Eq. (6):

$$\sigma_{spp} = \frac{KM}{(1-\nu)^{0.5}} \frac{Gb}{(\lambda_{spp}-d_{spp})} \quad [6]$$

where, K = 0.127 and Poisson's ratio ν = 0.31. The secondary phase particle strengthening contribution was thus calculated as σ_{spp} = 570 ± 110 MPa.

Intergranular coarse particle strengthening

The two intergranular phases in the present alloy are the Laves phase and the Cr_2O_3 oxides. These latter were

essentially located at the triple junctions of the γ grains, while the Laves phase was randomly distributed at the γ grain boundaries throughout the alloy. Both phases behave as intergranular chemically, crystallographic and mechanically alloy constituents different from the γ-phase. Thence, their strengthening contribution can be considered to act as a composite-like mechanism. While the Laves phase particles have a regular-solid geometric morphology, the Cr_2O_3 oxides have a spherical morphology. According to the shear-lag model proposed by Nardone and Prewo in [43], both the Laves phase particles and the Cr2O3 oxides reinforced the alloy by carrying a fraction of the load (load-transfer strengthening contribution, σ_{LT}) from the γ-phase (the matrix).

This strengthening contribution strongly depends on the morphology of the particles, namely, on their aspect ratio [42,43] as shown in Eq. (7a):

$$\sigma_{LT}^{particle} = \sigma_0 \left(1 + \frac{A(L+t)}{4L}\right) V_v^{particle} + \sigma_0 (1 - V_v^{particle}) \quad [7a]$$

where σ_0 is the matrix stress, which in this case is the HEA $\sigma_0 \cong 255$ MPa; V_v is the particle (Laves or Cr_2O_3) volume fraction; L is the particle size facing the load direction; t is the mean particle thickness; and A = L/t is the particle aspect ratio.

For geometrical but regular and slightly elongated Laves particles (L/t = 0.92), whose volume fraction, V_V = 25% (Table 2), Eq. (6a) can be rewritten as, Eq. (7b):

$$\sigma_{LT}^{Laves} = \sigma_0 (1.48) V_v^{Laves} + \sigma_0 (1 - V_v^{Laves}) \quad [7b]$$

For equiaxed particles, as in the case of the Cr_2O_3 oxide particles, Eq. (7a) reduces to Eq. (7c):

$$\sigma_{LT}{}^{Cr2O3} = 0.5 V_V{}^{Cr2O3} \sigma_0 \quad [7c]$$

The Cr_2O_3 volume fraction, $V_V{}^{Cr2O3}$, was estimated to be 3% (Table 2).

Thence, the Laves load transfer strengthening contribution accounted for $\sigma_{LT}{}^{Laves} = 285 \pm 10$ MPa, while the corresponding strengthening contribution from the Cr_2O_3 was $\sigma_{LT}Cr_2O_3 = 4 \pm 1$ MPa and thus negligible.

In general, the presence of sub-micrometre and micrometre particles also generates a microstructure mismatch due to the different thermal expansion coefficients (CTE) between the particles and the matrix. This, in turn, induces a dislocation density rise, yielding an additional strengthening contribution to the alloy, generally named the particle thermal expansion contribution, σ_{TE} [42,43]. This additional strengthening contribution was thus calculated by Eqs. (8a) and (8b):

$$\sigma_{TE}{}^{Cr2O3} = \alpha \mu G b (\rho_{Cr2O3\_thermal}{}^{0.5}) \quad [8a]$$

$$\sigma_{TE}{}^{Laves} = \alpha \mu G b (\rho_{Laves\_thermal}{}^{0.5}) \quad [8b]$$

This additional dislocation strengthening mechanism strongly depends on the particle geometry, namely on the particle surface-to-volume ratio (S/V). In the case of the spherical Cr_2O_3 oxides, $S/V = 6/d_{Cr2O3} = 8.6 \cdot 10^{-2}$ nm^{-1}. The Laves phases have a geometric morphology that is more similar to a parallelogram than a sphere, as in the case of the Cr_2O_3 oxides. Thus, for the Laves phase, their parallelogram-like morphology was assumed to be essentially cubic. Thus, according to the specific zone axis selected for the TEM inspections ($hcp_{1\text{-}100}$ and $hcp_{11\text{-}20}$ Laves zone axes), the quasi-cubic-like Laves phase had side $s = d_{Laves} \cdot \sqrt{2}$ and $S/V = 6/s = 7.1 \cdot 10^{-2}$ nm^{-1}. The calculated S/V ratio of the intergranular Cr_2O_3 oxide particles was ~17% larger than that of the intergranular Laves phase particles. Therefore, according to Eq. (7a) and (7b), the two thermal expansion strengthening terms were $\sigma_{TE}{}^{Cr2O3} = 280 \pm 60$ MPa and $\sigma_{TE}{}^{Laves} = 330 \pm 60$ MPa.

Therefore, the overall strengthening contribution yield by Cr_2O_3 oxide particles was $\sigma^{Cr2O3} = \sigma_{LT}^{Cr2O3} + \sigma_{TE}^{Cr2O3} \cong \sigma_{TE}^{Cr2O3} = 290 \pm 60$ MPa, while the one from Laves phase was $\sigma^{rLaves} = \sigma_{LT}^{Laves} + \sigma_{TE}^{Laves} = 620 \pm 70$ MPa.

Other possible strengthening contributions

The Laves phase particles were found to be nanometric with mean equivalent diameter $D_{Laves} = 120 \pm 20$ nm (Figure 4). The Laves particle strengthening contribution was modelled according to Eq. (9) [44,45]:

$$\sigma_{OR} = (Gb/\Lambda) + (5GV_V^{Laves}\varepsilon_p/2\pi) \quad [9]$$

where, Λ is the mean distance between the Laves particles, εp is the plastic strain. This strengthening contribution would be not significant as the mean distance between the Laves particles, Λ, is large.

Quite similar argument can be extended to the intergranular Cr_2O_3 oxide particles, which are even almost one-order of magnitude less abundant than the Laves phase.

Anyhow, Xie *et al.* [30,46] proposed a further strengthening contribution also acting by the presence of intergranular Laves particles, modelled through a modified Orowan-like mechanism, σ_{OR}^{mod}, by Eq. (10):

$$\sigma_{OR}^{mod} = \frac{\left(M\frac{0.4Gb}{\pi}\right)\frac{ln\left(\frac{(2/3)^{0.5}D^{Laves}}{b}\right)}{(1-\nu)^{0.5}}}{(2/3)^{0.5}D^{Laves}\left(\left(\pi/4V_v\right)^{0.5}-1\right)} \quad [10]$$

where, D^{Laves}, and V_V are, respectively, the mean size and volume fraction of the Laves phase. Thus, by taking the $D^{Laves} = 120 \pm 20$ nm and $V_V = 25 \pm 6\%$, $\sigma_{OR}^{mod} = 35 \pm 4$ MPa. This further contribution can be added to the overall Laves phase strengthening of $\sigma^{rLaves} = (\sigma_{LT}^{Laves} + \sigma_{TE}^{Laves}) + \sigma_{OR}^{mod} = 655 \pm 75$ MPa.

A similar contribution, could be in principle determined also for the intergranular Cr_2O_3 oxide particles, anyhow, their quite low volume fraction makes it as negligible factor.

Finally, In some of the γ-grains few small rounded secondary-particles were observed and identified as Cr_7C_3 carbides. The driving force to promote a fraction of the solute C in Cr_7C_3 carbide particles is given by the SPS process at 1273K. It resulted that the quite limited fraction of these carbides and their mean size make these particles not relevant by a strengthening contribution viewpoint, and thus it was not taken into account in the strengthening model here proposed.

HEA strengthening model

All the calculated microstructure strengthening terms were added to Eq. (1) to calculate the strengthening mechanism of the sub-micrometre-grained equiatomic CoCrFeNiNb HEA. This microstructure strengthening model was compared to the ultimate compression strength, UCS, (Table 2). Thence, according to the Eq. (1), the modelled strength of the CoCrFeNiNb HEA is, Eq. (11):

$$\sigma_y^{model} = \sigma_0 + \sigma_{ss} + \sigma_d + \sigma_{HP} + \sigma_T + \sigma_{ssp} + \sigma_P$$
$$= \sigma_0 + \{[V_V^{\gamma}(\sigma_{ss}+\sigma_d+\sigma_{HP}+\sigma_{spp}+\sigma_T)]^2 + [V_V^{Laves}(\sigma_{TE}^{Laves}+\sigma_{LT}^{Laves}) + V_V^{Cr2O3}(\sigma_{TE}^{Cr2O3})]^2\}^{0.5} = 1995 \text{ MPa.} \quad [11]$$

This mean value is only 13% lower than the value experimentally measured of $\sigma_y^{exp} = 2291$ MPa at room temperature.

Thus, the proposed microstructure-based model reasonably agreed with the experimental results for the alloy compression strength at room temperature. The most relevant strengthening contribution can be identified as the γ phase and related microstructure features (Hall-Petch, twinning, tangled dislocations, and secondary-phase particles). The strengthening contribution of the Laves phase was composite-type, as well as that of the few Cr_2O_3 oxides. The little discrepancy from the model and the experimentally-derived HEA yield compression strength might be due to a different Hall-Petch constant, k_{HP}, which possibly be more appropriate in the specific case of the here studied equiatomic HEA modelled by room-temperature

compression test. As already reported, different k_{HP} values were proposed, and in some cases these were higher than the one here used k_{HP} = 400 MPa·μm$^{1/2}$. This would rise to some 5-to-8% the alloy yield compression stress as obtained by the microstructure model, and thus approaching the model-based yield strength to the experimentally based one.

On the other hand, the microstructure model reported here well agrees with similar proposed models and related findings recently published by Fu *et al.* in [47]. In their study, they attributed the major strengthening contributions to the yield stress to the FCC phase grain boundaries and tangled dislocations in a $Co_{25}Ni_{25}Fe_{25}Al_{7.5}Cu_{17.5}$ HEA.

Tab.2 - Experimental data and microstructure strengthening contributions for the 8h MA+SPS alloy compacted at 1273K as calculated by Eq.(1).

V_V	γ phase 0.72 ± 0.07	Laves 0.25 ± 0.06	Cr_2O_3 0.03 ± 0.01	σ^{min}, MPa	σ^{max}, MPa	σ^{mean}, MPa
ρd, 10^{15} m^{-2}	0.70 ± 0.1	-	-	290	330	**310**
λ_{TB}, nm	11.0 ± 2.5	-	-	300	380	**340**
Dγ, nm	180 ± 45	-	-	740	940	**830**
d_{spp}, nm	7.5 ± 0.5	-	-			
λ_{spp}, nm	23 ± 3	-	-	460	680	**570**
V_v^{spp} of $V_v^{\gamma\ phase}$, %	1.4 ± 0.2	-	-			
D_{Laves}, nm	-	120 ± 20	-	580	730	**655**
D_{Cr2O3}, nm	-	-	70 ± 20	230	350	**290**
				1700	2325	**1995**

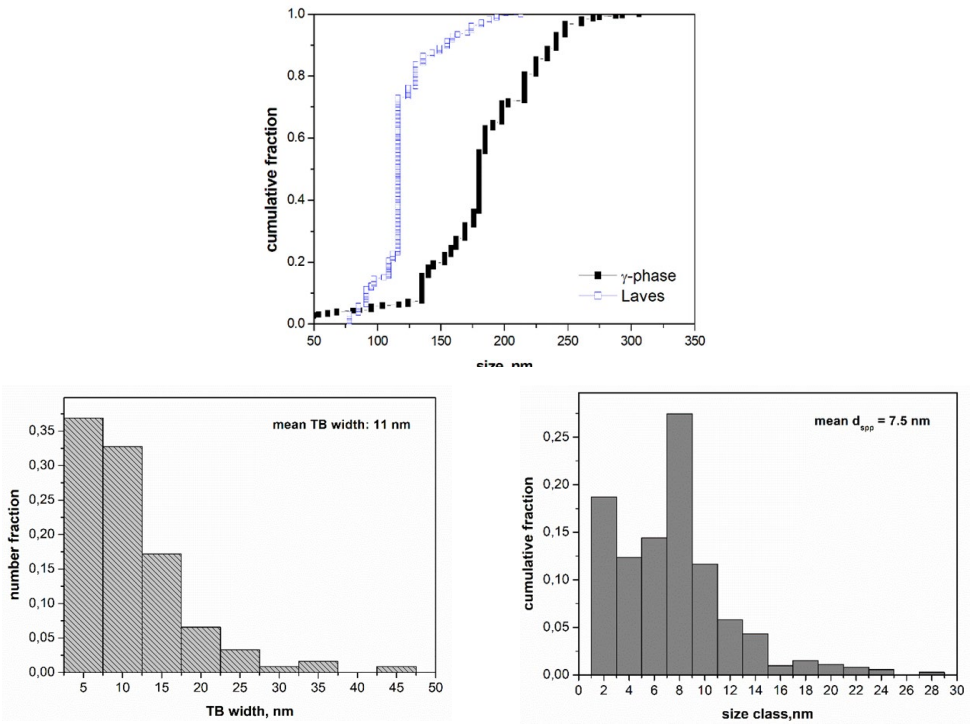

Fig.3 - Statistical evaluation of microstructure parameters used to calculate the different microstructure strengthening terms through Eqs. (2)-(10) for the 8h MA+SPS alloy compacted at 1273K showing: a) grain size cumulative distribution of both γ-phase, d_g^{γ} and Laves phase, d_g^{Laves}; b) distribution of the twin boundary spacing, λ_{TB}; c) size distribution of second-phase particles within the γ-phase, d_{spp}.

Thus, a simpler strengthening model including the solid-solution, grain boundary, secondary-phase particles, and stacking-faults (SF) strengthening terms, proposed by Zhao *et al.* [48], was able to account for the mechanical response of a CoCrNi medium-entropy alloy (MEA) to some extent. In this latter case, in addition to the FCC phase grain boundary, a significant strengthening contribution was given by the SFs within the FCC phase. The key role of the SFs was also reported in two HEAs, i.e., AlCoCrCuFeNi by Ganji *et al.* [49] and CoCrFeMnNi by Laurent-Brocq *et al.* [50], although in the latter case, the role of the SFs was indirectly inferred by modelling the alloy hardness.

Similar microstructure strengthening models were proposed in other recent publications [51-53]. In particular, Tong *et al.* [51] identified essentially the same microstructure contributions to model the tensile stress of a non-equiatomic $FeCoNiCrTi_{0.2}$ HEA. In that study, solid solution strengthening and secondary-phase particles within fcc grains, and both coherent and anti-phase boundary energy, were considered. SF energy accounted for a significant fraction of the alloy stress, which is in good agreement with the present findings.

Gao *et al.* [52] recognized three major strengthening contributions in a CrMnFeCoNi HEA: fcc grain refinement (Hall-Petch), precipitation strengthening and tangled dislocations within the fcc phase. Similarly, Kang *et al.* [53] modelled the compressive yield stress of a WNbMoTaV HEA and identified similar strengthening contributions of the ones described here. In their work, they found quite high compression yield stress, σ_y = 2618 MPa. This exceptionally high value was essentially attributed to the fcc grain boundary strengthening, and specifically by solid solution and existing secondary-phase particle Orowan strengthening.

The rule of mixtures and summation of the different microstructure strengthening phases that was proposed herein is in good agreement with the works by Huo *et al.* [54] for a CoCrFeNiTa HEA and by Stepanov *et al.* [55] for ($AlCr_{x=0.5/1.0/1.5}NiTiV$) different HEAs used a partitioning approach for the different phase volume fractions.

Finally, a quadratic sum of the different types of contributions was extensively justified and discussed in a previous published work by Cabibbo [20].

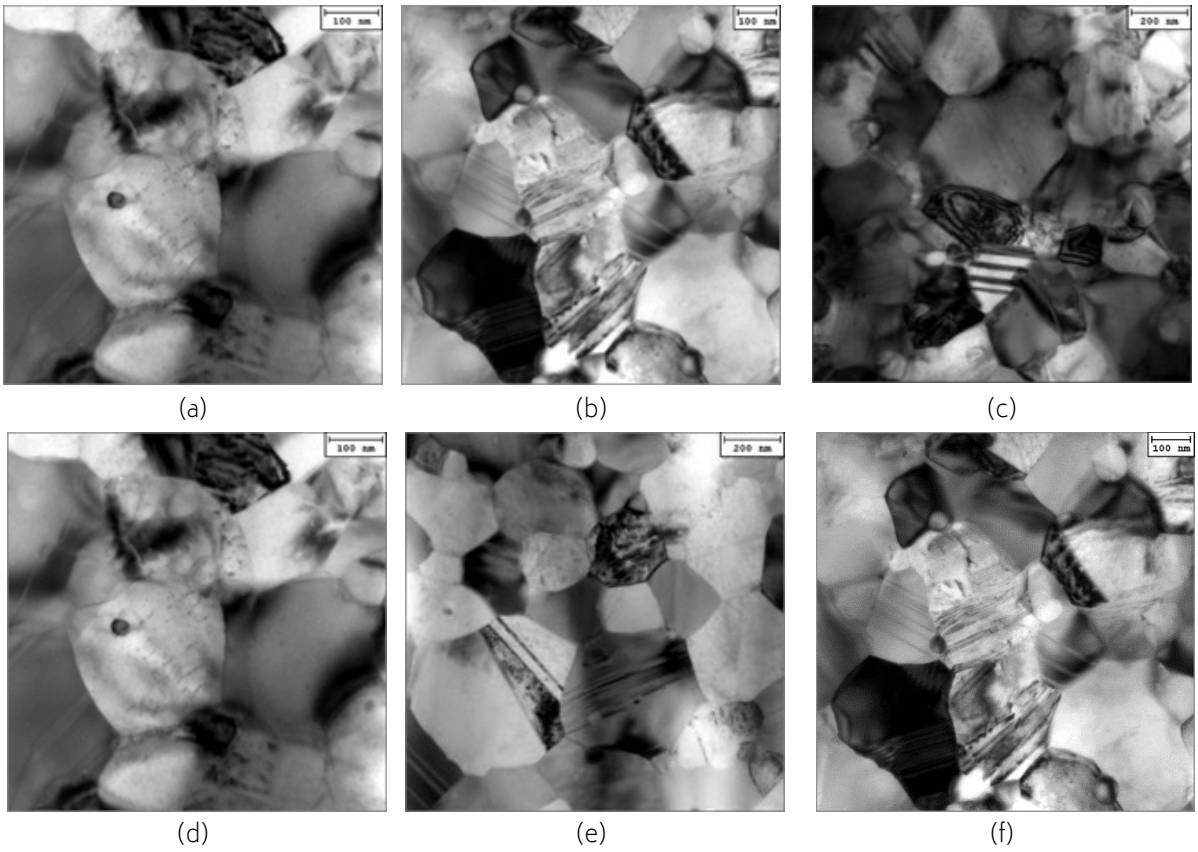

Fig.4 - BF-TEM representative micrographs showing the typical microstructure strengthening mechanisms including: a) dislocation strengthening within the γ-phase, ρ_d; b) typical size of both γ and Laves phases, d_g^{γ}, and d_g^{Laves}; c) typical twin boundary morphology and spacing, λ_{TB}, within the γ-phase; d) a representative micrograph showing the typical size of Cr_7C_3 carbides within the γ-grains; in e), typical size of the intergranular rounded Cr_2O_3; in f), BF-TEM displaying the three existing alloy constituents: γ-phase, Laves, Cr_2O_3.

CONCLUSIONS

The equiatomic CoCrFeNiNb alloy was prepared by a combination of MA+SPS yielding a sub-micrometer grain refinement. The initial microstructure consisted of sub-micrometer γ-phase grains, intergranular sub-micrometer Laves phase particles and nanocrystalline intergranular Cr_2O_3 oxides. The MA+SPS alloy compacted at 1273 K showed exceptional compressive properties, reaching an ultimate compression strength of 2412 MPa. These excellent properties were chiefly due to a refined microstructure characterized by the formation of stacking faults and deformation nano-twins, and the presence of composite-like structures composed by Laves and Cr_2O_3 oxides. The results of the compressive tests were in good agreement with the microstructure strengthening model based on quantitative TEM analyses. It was found that the highest contribution was given by fcc γ-phase solid solution. Thermal stability was guaranteed by the presence of both intergranular Laves and oxide particles that hindered γ-phase grain growth upon compression at high temperature.

ACKNOWLEGEMENTS

This work was supported by the specific university research (MSMT No 21-SVV/2019).

REFERENCES

[1] B. Cantor, I.T.H. Chang, P. Knight, A.J.B. Vincent, Microstructural development in equiatomic multicomponent alloys, Mater. Sci. Eng. A. 375-377 (2004) 213-218.
[2] Y. Yu, F. He, Z. Qiao, Z. Wang, W. Liu, J. Yang, Effects of temperature and microstructure on the triblogical properties of CoCrFeNiNbx eutectic high entropy alloys, J. All. Compd. 775 (2019) 1376-1385.
[3] M. Vaidya, G.M. Muralikrishna, B.S. Murty, High-entropy alloys by mechanical alloying: A review, J. Mater. Res. 34 (2019) 664-686.
[4] F. He, Z. Wang, P. Cheng, Q. Wang, J. Li, Y. Dang, J. Wang, C.T. Liu, Designing eutectic high entropy alloys of CoCrFeNiNbx, J. All. Compd. 656 (2016) 284-289.
[5] J. Joseph, N. Haghdadi, K. Shamlaye, P. Hodgson, M. Barnett, D. Fabijanic, The sliding wear behaviour of CoCrFeMnNi and AlxCoCrFeNi high entropy alloys at elevated temperatures, Wear 428-429 (2019) 32-44.
[6] Y. Zhang, X. Yang, P.K. Liaw, Alloy Design and Properties Optimization of High-Entropy Alloys, JOM. 64 (2012) 830-838.
[7] D.B. Miracle, O.N. Senkov, A critical review of high entropy alloys and related concepts, Acta Mater. 122 (2017) 448-511.
[8] S.G. Ma, Y. Zhang, Effect of Nb addition on the microstructure and properties of AlCoCrFeNi high-entropy alloy, Mater. Sci. Eng. A. 532 (2012) 480-486.
[9] G. Qin, S. Wang, R. Chen, X. Gong, L. Wang, Y. Su, J. Guo, H. Fu, Microstructures and mechanical properties of Nb-alloyed CoCrCuFeNi high-entropy alloys, J. Mater. Sci. Technol. 34 (2018) 365-369.
[10] H. Jiang, L. Jiang, D. Qiao, Y. Lu, T. Wang, Z. Cao, T. Li, Effect of Niobium on Microstructure and Properties of the CoCrFeNbxNi High Entropy Alloys, J. Mater. Sci. Technol. 33 (2017) 712-717.
[11] F. He, Z. Wang, X. Shang, C. Leng, J. Li, J. Wang, Stability of lamellar structures in CoCrFeNiNbx eutectic high entropy alloys at elevated temperatures, Mater. Design 104 (2016) 259-264.
[12] B. Liu, J. Wang, Y. Liu, Q. Fang, Y. Wu, S. Chen, C.T. Liu, Microstructure and mechanical properties of equimolar FeCoCrNi high entropy alloy prepared via powder extrusion, Intermetallics 75 (2016) 25-30.
[13] M. Vaidya, A. Karati, A. Marshal, K.G. Pradeep, B.S. Murty, Phase evolution and stability of nanocrystalline CoCrFeNi and CoCrFeMnNi high entropy alloys, J. All. Compd. 770 (2019) 1004-1015.
[14] F. Průša, A. Šenková, V. Kučera, J. Čapek, D. Vojtěch, Properties of a high-strength ultrafine-grained CoCrFeNiMn high-entropy alloy prepared by short-term mechanical alloying and spark plasma sintering, Mater. Sci. Eng. A. 734 (2018) 341-352.
[15] J. C. Russ, R., T. Dehoff, Practical Stereology, 2nd Ed. Springer Science & Business Media LLC New York, USA, 2000.
[16] F. He, Z. Wang, Q. Wu, D. Chen, T. Yang, J. Li, J. Wang, C.T. Liu, J.-j. Kai, Tuning the defects in face centered cubic high entropy alloy via temperature-dependent stacking fault energy, Scripta Mater. 155 (2018) 134-138.
[17] Ł. Rogal, D. Kalita, A. Tarasek, P. Bobrowski, F. Czerwinski, Effect of SiC nanoparticles on microstructure and mechanical properties of the CoCrFeMnNi high entropy alloy, J. All. Compd. 708 (2017) 344-352.
[18] W.H. Liu, T. Yang, and C.T. Liu, Precipitation hardening in CoCrFeNi-based high entropy alloys, Mater. Chem. Phys. 210 (2018) 2-11.
[19] A.I.H. Committee, Properties and Selection: Nonferrous Alloys and Special-Purpose Materials, 1990.

[20] M. Cabibbo, Microstructure strengthening mechanisms in different equal channel angular pressed aluminum alloys, Mater. Sci. Eng., A. 560 (2013) 413-432. https://doi.org/10.1016/j.msea.2012.09.086
[21] J.Y. He, W.H. Liu, H. Wang, Y. Wu, X.J. Liu, T.G. Nieh, Z.P. Lu, Effects of Al addition on structural evolution and tensile properties of the FeCoNiCrMn high-entropy alloy system, Acta Mater. 62 (2014) 105-113.
[22] I. Toda-Caraballo, P.E.J. Rivera-Díaz-del-Castillo, Modelling solid solution hardening in high entropy alloys, Acta Mater. 85 (2015) 14-23.
[23] J.Y. He, H. Wang, H.L. Huang, X.D. Xu, M.W. Chen, Y. Wu, X.J. Liu, T.G. Nieh, K. An, Z.P. Lu, A precipitation-hardened high-entropy alloy with outstanding tensile properties, Acta Mater. 102 (2016) 187-196.
[24] T.H. Courtney, Mechanical Behavior of Materials: Second Edition, Waveland Press Inc., Long Grove, Illinois, USA, 2005.
[25] C. Zhu, Z.P. Lu, and T.G. Nieh, Incipient plasticity and dislocation nucleation of FeCoCrNiMn high-entropy alloy, Acta Mater. 61 (2013) 2993-3001.
[26] D. Shaysultanov, N. Stepanov, S. Malopheyev, I. Vysotskiy, V. Sanin, R. Kaibyshev, G. Salishchev, S. Zherebtsov, Friction stir welding of a carbon-doped CoCrFeNiMn high-entropy alloy, Mater. Character. 145 (2018) 353-361.
[27] A. Heczel, M. Kawasaki, J.L. Labar, J.-il Jang, T.G. Langdon, J. Gubicza, Defect structure and hardness in nanocrystalline CoCrFeMnNi High Entropy Alloy processed by High-Pressure Torsion, J. All. Compd. 711 (2017) 143-154.
[28] M. Klimova, N. Stepanov, D. Shaysultanov, R. Chernichenko, N. Yurchenko, V. Sanin, S. Zherebtsov, Microstructure and Mechanical Properties Evolution of the Al, C-Containing CoCrFeNiMn-Type High-Entropy Alloy during Cold Rolling, Metals 11 (2018) 53-61.
[29] Z.G. Zhu, Q.B. Nguyen, F.L. Ng, X.H. An, X.Z. Liao, P.K. Liaw, S.M.L. Nai, J. Wei, Hierarchical microstructure and strengthening mechanisms of a CoCrFeNiMn high entropy alloy additively manufactured by selective laser melting, Scripta Mater. 154 (2018) 20-24.
[30] Y. Xie, Y. Luo, T. Xia, W. Zeng, J. Wang, J. Liang, D. Zhou, D. Zhang, Grain growth and strengthening mechanisms of ultrafine-grained CoCrFeNiMn high entropy alloy matrix nanocomposites fabricated by powder metallurgy, J. All. Compd. 819 (2020) 152937.
[31] F. Průša, A Šenková, V. Kučera, J. Čapek, D. Vojtěch, Properties of a high-strength ultrafine-grained CoCrFeNiMn high-entropy alloy prepared by short-term mechanical alloying and spark plasma sintering, Mater. Sci. Eng. A 734 (2018) 341-352.
[32] S.J. Sun, Y.Z. Tian, H.R. Lin, H.J. Yang, X.G. Dong, Y.H. Wang, Z.F. Zhang, Transition of twinning behavior in CoCrFeMnNi high entropy alloy with grain refinement, Mater. Sci. Eng. A 712 (2018) 603-607.
[33] S.J. Sun, Y.Z. Tian, H.R. Lin, X.G. Dong, Y.H. Wang, Z.J. Zhang, Z.F. Zhang, Enhanced strength and ductility of bulk CoCrFeMnNi high entropy alloy having fully recrystallized ultrafine-grained structure, Mater. & Design 133 (2017) 122-127.
[34] F. Otto, A. Dlouhy, Ch. Somsen, H. Bei, G. Eggeler, E.P. George, The influences of temperature and microstructure on the tensile properties of a CoCrFeMnNi high-entropy alloy, Acta Mater. 61 (2013) 5743-5755.
[35] D.G. Kim, Y.H. Jo, J.M. Park, W.-M. Choi, H.S. Kim, Effects of annealing temperature on microstructures and tensile properties of a single FCC phase CoCuMnNi high-entropy alloy, J. All. Compd. 812 (2020) 152111.
[36] Y.L. Zhao, T. Yang, Y. Tong, J. Wang, J.H. Luan, Z.B. Jiao, D. Chen, A. Hu, C.T. Liu, J.-J. Kai, Y. Yang, Heterogeneous precipitation behavior and stacking-fault-mediated deformation in a CoCrNi-based medium-entropy alloy, Acta Mater. 138 (2017) 72-82.
[37] S.J. Sun, Y.Z. Tian, H.R. Lin, X.G. Dong, Y.H. Wang, Z.J. Wang, Z.F. Zhang, Temperature dependence of the Hall-Petch relationship in CoCrFeMnNi high-entropy alloy, J. All. Compd. 806 (2019) 992-998.
[38] K. Cho, Y. Fujioka, T. Nagase, H.Y. Yasuda, Grain refinement of non-equiatomic Cr-rich CoCrFeMnNi high-entropy alloys through combination of cold rolling and precipitation of σ phase, Mater. Sci. Eng. A 735 (2018) 191-200.
[39] N. Stepanov, M. Tikhonovsky, N. Yurchenko, D. Zyabkin, S. Zherebtsov, A. Efimov, G. Salishchev, M. Klimova, Effect of cryo-deformation on structure and properties of CoCrFeNiMn high-entropy alloy, Intermetallics 59 (2015) 8-17.
[40] W.H. Liu, Y. Wu, J.Y. He, T.G. Nieh, Z.P. Lu, Grain growth and the Hall–Petch relationship in a high-entropy FeCrNiCoMn alloy, Scripta Mater. 68 (2013) 526-529.
[41] X. Li, Y. Wei, L. Lu, K. Lu, H. Gao, Dislocation nucleation governed softening and maximum strength in nano-twinned metals, Nature. 464 (2010) 877.
[42] M. Cabibbo and S. Spigarelli, A TEM quantitative evaluation of strengthening in an Mg–RE alloy reinforced with SiC, Mater. Character. 62 (2011) 959-969.
[43] V.C. Nardone, K.M. Prewo, On the strength of discontinuous silicon carbide reinforced aluminum composites, Scripta Metall. 20 (1986) 43-48.
[44] Z. Trojanová, Z. Drozd, S. Kudela, Z. Száraz, P. Lukáč, Strengthening in Mg-Li matrix composites, Comp. Sci. Technol. 67 (2007) 1965-1973.
[45] I. Moravcik, L. Gouvea, V. Hornik, Z. Kovacova, M. Kitzmantel, E. Neubauer, I. Dlouhy, Synergic strengthening by oxide and coherent precipitate dispersions in high-entropy alloy prepared by powder metallurgy, Scripta Mater. 157 (2018) 24-29.
[46] Y. Xie, D. Zhou, Y. Luo, T. Xia, Z. Weng, C. Li, J. Wang, J. Liang, D. Zhang, Fabrication of CoCrFeNiMn high entropy alloy matrix composites by thermomechanical consolidation of a mechanically milled powder, Mater. Character. 148 (2019) 307-316.
[47] Z. Fu, W. Chen, H. Wen, D. Zhang, Z. Chen, B. Zheng, Y. Zhou, E.J. Lavernia, Microstructure and strengthening mechanisms in an FCC structured single-phase nanocrystalline Co25Ni25Fe25Al7.5Cu17.5 high-entropy alloy, Acta Mater. 107 (2016) 59-71.
[48] Y.L. Zhao, T. Yang, Y. Tong, J. Wang, J.H. Luan, Z.B. Jiao, D. Chen, Y. Yang, A. Hu, C.T. Liu, J.J. Kai, Heterogeneous precipitation behavior and stacking-fault-mediated deformation in a CoCrNi-based medium-entropy alloy, Acta Mater. 138 (2017) 72-82.
[49] R.S. Ganji, P. Sai Karthik, K. Bhanu Sankara Rao, K.V. Rajulapati, Strengthening mechanisms in equiatomic ultrafine grained

AlCoCrCuFeNi high-entropy alloy studied by 36 micro- and nanoindentation methods, Acta Mater. 125 (2017) 58-68.
[50] M. Laurent-Brocq, P.A. Goujon, J. Monnier, B. Villeroy, L. Perrière, R. Pirès, and G. Garcin, Microstructure and mechanical properties of a CoCrFeMnNi high entropy alloy processed by milling and spark plasma sintering, J. Alloys Compd. 780 (2019) 856-865.
[51] Y. Tong, D. Chen, B. Han, J. Wang, R. Feng, T. Yang, C. Zhao, Y.L. Zhao, W. Guo, Y. Shimizu, C.T. Liu, P.K. Liaw, K. Inoue, Y. Nagai, A. Hu, J.J. Kai, Outstanding tensile properties of a precipitation-strengthened FeCoNiCrTi0.2 high-entropy alloy at room and cryogenic temperatures, Acta Mater. 165 (2019) 228-240.
[52] N. Gao, D.H. Lu, Y.Y. Zhao, X.W. Liu, G.H. Liu, Y. Wu, G. Liu, Z.T. Fan, Z.P. Lu, E.P. George, Strengthening of a CrMnFeCoNi high-entropy alloy by carbide precipitation, J. Alloys Compd. 792 (2019) 1028-1035.
[53] B. Kang, J. Lee, H.J. Ryu, and S.H. Hong, Ultra-high strength WNbMoTaV high-entropy alloys with fine grain structure fabricated by powder metallurgical process, Mater. Sci. Eng. A. 712 (2018) 616-624.
[54] W. Huo, H. Zhou, F. Fang, X. Zhou, Z. Xie, J. Jiang, Microstructure and properties of novel CoCrFeNiTax eutectic high-entropy alloys, J. Alloys Compd. 735 (2018) 897-904.
[55] N.D. Stepanov, N.Y. Yurchenko, D.V. Skibin, M.A. Tikhonovsky, G.A. Salishchev, Structure and mechanical properties of the AlCrxNbTiV (x = 0, 0.5, 1, 1.5) high entropy alloys, J. All. Compd. 652 (2015) 266-280.